Application of Ultra-Wideband Sensors for On-Line Monitoring of Transformer Winding Radial Deformations–A Feasibility Study

Maryam Sadat Akhavan Hejazi, Javad Ebrahimi, *Student Member, IEEE*, Gevork B. Gharehpetian, *Senior Member, IEEE*, Mohammad Mohammadi, Reza Faraji-Dana, and Gholamreza Moradi

***Abstract*— A new method for the on-line monitoring of transformer winding radial deformations using ultra-wideband sensors is presented in this paper. A wideband signal is sent to a simplified model of the transformer winding. The measurements of received signals from the model winding demonstrate the sensitivity of the proposed technique to the winding radial deformation. It is shown that the deformation volume can be estimated using a proposed index. Also, the amount of the radial deformation is estimated by using a regression tree based on features extracted by the wavelet transform.**

***Index Terms*— Condition monitoring, decision trees, discrete wavelet transforms, nondestructive testing, power transformers, time of arrival estimation, ultra wideband antennas, ultra wideband radar.**

I. Introduction

MONITORING of electric machines for the detection of electrical and mechanical faults have been widely used for extending their life expectancy [1]. Power transformers are one of the most expensive and highly essential electric machinery in the electric power systems whose failures and abnormal operations may lead to the outage of a power system.

As a transformer ages, its internal condition degrades, which increases the risk of failure [2]. The short circuits due to electrodynamics forces cause radial deformations and axial displacements of transformer windings. These mechanical damages may not lead to an immediate failure of the transformer, but the ability of the transformer to withstand future mechanical and dielectric stresses may be highly decreased [3], [4].

Manuscript received May 31, 2011; revised October 19, 2011; accepted October 27, 2011. Date of publication November 9, 2011; date of current version April 20, 2012. The work was financially supported by Tehran Regional Electric Company. The associate editor coordinating the review of this paper and approving it for publication was Dr. Dwight L. Woolard.

M. A. Hejazi, J. Ebrahimi, G. B. Gharehpetian, and G. Moradi are with the Center of Excellence on Power Systems, Electrical Engineering Department, Amirkabir University of Technology, Tehran 15914, Iran (e-mail: akhavanhejazi@gmail.com; j_ebrahimi@aut.ac.ir; grptian@aut.ac.ir; ghmoradi@aut.ac.ir).

M. Mohammadi is with the School of Electrical and Computer Engineering, Shiraz University, Shiraz 71345, Iran (e-mail: m.mohammadi@aut.ac.ir).

R. Faraji-Dana is with the Center of Excellence on Applied Electromagnetic Systems, School of Electrical and Computer Engineering, College of Engineering, University of Tehran, Tehran 14174, Iran (e-mail: reza@ut.ac.ir).

Color versions of one or more of the figures in this paper are available online at http://ieeexplore.ieee.org.

Digital Object Identifier 10.1109/JSEN.2011.2175723

The requirement of safe and reliable operation of power transformers leads to study and development of several fault detection and conditions monitoring methods. Each method can be applied to a specific type of problem and has its own advantages and disadvantages [5], [6]. In recent years, several off-line methods such as Short Circuit test method (SC) [3], Low Voltage Impulse method (LVI) [7] and Frequency Response Analysis method (FRA) [5] for the detection of the winding deformation have been proposed. In SC test method, the short circuit reactance is measured while the transformer is off-line. In this method, the sensitivity of the reactance to the winding displacement is very low, and the type and the location of the mechanical damage in the winding cannot be determined [5].

In the FRA method, experimental approaches of comparison are: time-based, type-based and construction-based. A prerequisite of all three methods is the independency of the measurement from the setup to create reproducible results. The FRA method can be used off-line and on-line [8], [9]. The well-known FRA method has been carried out off-line. In the off-line FRA method, the transformer is switched on and off, on the high voltage side (HV-side). Therefore, the transformer is disconnected from the power network on the low voltage side (LV-side) [8].

In the on-line FRA method, the frequency response should be measured during the operation of the transformer. The stochastic transient over-voltages caused by the switching and the lightning can be used to determine the transfer function. Many factors affect this method such as response of arresters and different power system topologies. The measurement timing depends on the time of occurrence of overvoltage transients [10]. The on-line FRA method is in the research phase and has not been used for any transformer.

The off-line methods do not meet all the needs of the transformer monitoring systems. The on-line methods do not require switching of the transformer and can continuously monitor the transformer winding. The other advantage of the on-line monitoring method is the prediction of important faults before their occurrence [11].

The simulations have shown that the scattering parameter of the winding can be used as an index for on-line monitoring of winding radial and axial deformations [12], [13]. The same as FRA method, this method is based on the comparison of

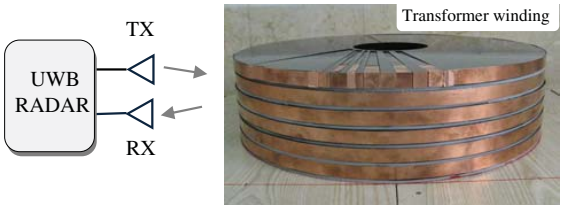

Fig. 1. Basic principle of monitoring by using UWB radar sensor.

results. In this method, the scattering parameters are used as a fingerprint for the transformer winding [14]–[16]. This method is also in the research phase and has not been used for any transformer.

In this paper, a new Nondestructive testing method of the transformer winding damages has been developed using the high frequency electromagnetic waves analysis in the time domain. The proposed method has been tested on a model of transformer for different volumes of radial deformation. The ultra-wideband (UWB) signals used for this method have very high accuracy for fault detection and can give more information about the type and location of the fault because of special characteristics of UWB signals.

According to the U.S. Federal Communications Commission (FCC), a UWB signal is defined to have an absolute bandwidth of at least 500 MHz or a fractional (relative) bandwidth of larger than 20% [17]. Large bandwidths of UWB signals bring many advantages such as penetration through obstacles, accurate position estimation, high-speed data transmission and low cost and low power transceiver designs [18]. The penetration capability of a UWB signal is due to its large frequency spectrum that includes low frequency components as well as high frequency ones. This large spectrum also results in high time resolution, which improves ranging (i.e., distance estimation) accuracy. From a radar viewpoint, short-pulse UWB techniques exhibit distinct advantages over more conventional radar approaches [19], [20]. Numerous applications of short-pulse technology were developed for short-range radar sensing, subsurface sensing [21], metrology, communications, and more recently, precision positioning [22] and radar imaging [23]. For active Radio Frequency (RF) tracking and positioning applications, short-pulse UWB techniques offer distinct advantages in precision time-of-flight measurement, multipath immunity for leading edge detection [i.e., first time of arrival (TOA)] and low prime power requirements for extended-operation RF identification (RFID) tags [24]. In this research, UWB pulses have been used for on-line monitoring of transformer winding mechanical damages, which can be considered as a slowly moving or stationary target.

II. Proposed Monitoring Method Using UWB Sensors

High frequency antennas have been used to monitor the partial discharge in the transformer [25]. The Ultra High Frequency (UHF) sensors of the partial discharge detection system work only in the receiving mode [25], [26]. These antennas can be placed inside or outside the transformer tank, through the dielectric windows, which have been recently

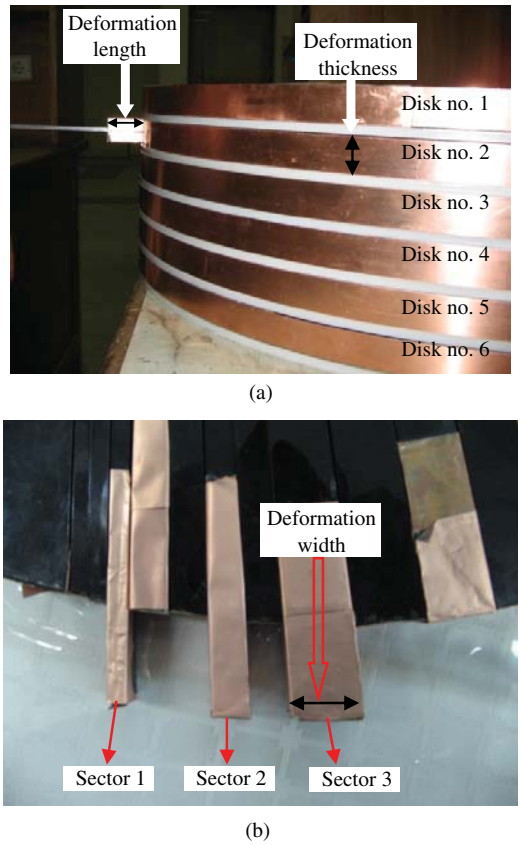

Fig. 2. Modeling of radial deformation. (a) Disk numbering and deformation length and thickness. (b) Deformation width.

designed as a solution for receiving the signals from the inside of transformer. The fundamental of the proposed method is based on UWB radar sensor. As shown in Fig. 1, the UWB radar generates short pulses and transmits them through the transmitting antenna (TX).

The signal propagates in an environment (transformer oil). When it meets target (transformer winding), a part of the electromagnetic energy is reflected from the object and propagates back to the receiving antenna (RX). It has been shown by simulations and measurements that the received waveforms are sensitive to winding axial displacements and radial deformations [27]–[29]. The proposed approach for interpreting the received signals is based on comparison. The waveform of the received signals can be used as a fingerprint of the transformer. The best way of comparison, like the FRA method, is time-based. The signal received from a healthy transformer can be stored in a database. The transformer can be monitored on-line in any time. If all of the parameters in the test, *e.g.* the antenna, transmitter and receiver characteristics and the antenna location, remain constant, then every deviation in the received signal from the healthy fingerprint of the transformer is only due to the mechanical changes in the environment of the wave propagation.

III. Measurement Method

A simplified model of transformer HV winding with the ability of modeling the axial displacement and radial defor-

TABLE I
DISK MODEL DIMENSIONS

	Disk	Spacer
Diameter	60 cm	60 cm
Thickness	2 cm	0.5 cm
Number	6	6

TABLE II
SECTORS DIMENSIONS

Deformation parameters	Sector 1	Sector 2	Sector 3
Width (cm)	0.5	1	2
Thickness (cm)	2	2	2
Area (cm^2)	1	2	4

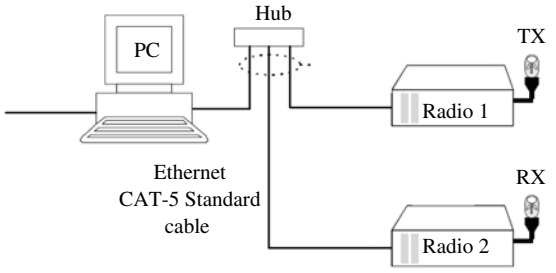

Fig. 3. Connection diagram of measurement set-up.

mation has been built, as shown in Figs. 1 and 2. This model should represent HV winding disks of transformers. Dimensions of the model are approximately 1/3 of a real one. Disks have been made from Plexiglas sheets which are covered by a layer of copper. It should be mentioned that the high frequency electromagnetic waves are totally reflected in the metal-air interface, so it is not necessary to model the core that is inside the windings. Disks are separated from each other by spacers, which have equal thickness. Table I lists the model dimensions.

One of these disks has been cut in sectors with different dimensions. These sectors can be moved in radial direction as shown in Fig. 2.

The amount of the deformation is characterized by the deformation length. The thickness of each sector is equal to the thickness of each disk. But their widths are different, as listed in Table II, in order to model different radial deformations.

In the oil-immerged power transformers, the oil is the propagation medium. In this paper, the propagation medium is considered to be air and the transformer tank is not modeled, and the radial deformation of only one phase of the transformer has been studied. It is assumed that there is not any high frequency source of electromagnetic waves in the transformer except the transmitter.

This method which is based on the comparison of results in different time periods is not sensitive to the environmental change such as humidity and temperature. It is because variation of humidity, in a maintenance period for an installed transformer is negligible and it is possible to measure only in a known winding temperature range.

A bi-static transmitter and receiver have been used for the measurements as shown in Fig. 3. The transmitter and receiver

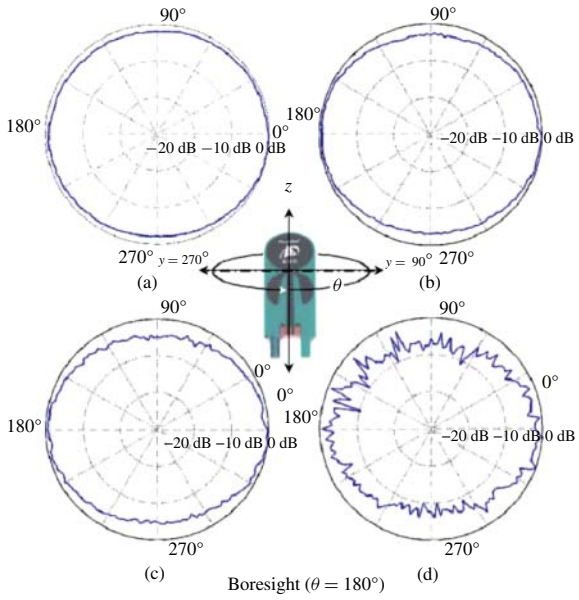

Fig. 4. Antenna horizontal radiation pattern. (a) 3 GHz. (b) 4 GHz. (c) 5 GHz. (d) 6 GHz.

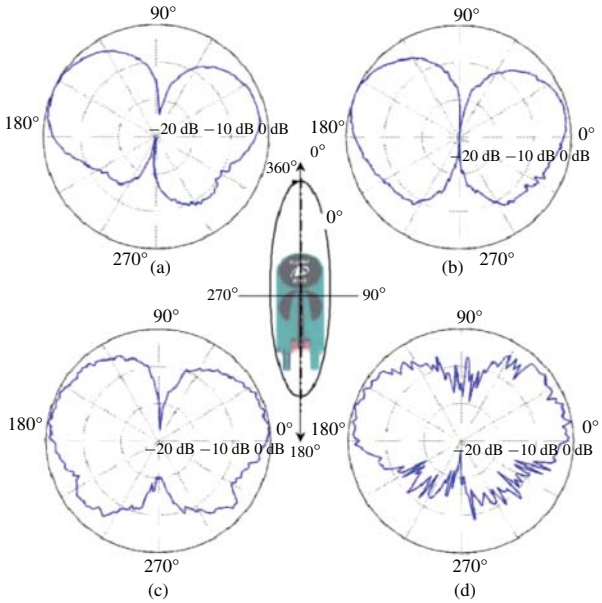

Fig. 5. Antenna vertical radiation pattern. (a) 3 GHz. (b) 4 GHz. (c) 5 GHz. (d) 6 GHz.

are connected via Ethernet CAT-5 standard cable to a hub and a PC. The received signals are stored in a text file.

Two UWB antennas have been used for the measurements. The antenna pattern is omni-directional. Fig. 4 shows the antenna azimuthal beam pattern, and Fig. 5 illustrates the elevation beam pattern. For the azimuthal beam pattern, 0 and 180 degrees represent the flat face of the antenna ("bore sight"), and 90 and 270 degrees represent the edge of the antenna. When two radios at the same elevation are rotated so the flat sides of the antennas face one another, due to the polarization of antennas, radio performance will be approximately 6 dB higher than the case, in which the antennas are edge-on.

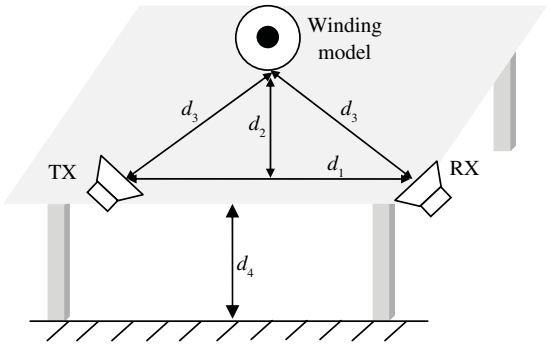

Fig. 6. Winding model in front of transmitting and receiving antennas.

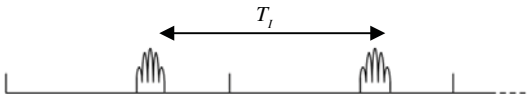

Fig. 7. Transmitted UWB pulses (every T_I seconds).

TABLE III
PARAMETERS OF TRANSMITTED PULSE

Maximum pulse repetition frequency (PRF)	9.6 MHz
Center frequency (radiated)	4.7 GHz
Bandwidth (10 dB radiated)	3.2 GHz
Power consumption	5.7 Watts

Fig. 6 shows the winding model in front of transmitting and receiving antennas. In this figure, d_1 is the distance between the transmitting and receiving antenna, d_2 is the distance between the winding model and the center of the line connecting the antennas, d_3 is the distance between the transmitting/receiving antennas from the model and d_4 is the height of the set-up table from the ground. It should be mentioned that the effect of changing the position of transmitter and receiver antennas on the detection of mechanical damages has been studied in [30] as a sensitivity analysis.

As shown in Fig. 7, UWB pulses are radiated to the transformer model from the transmitter every T_I seconds. The T_I parameter should be set lower for the detection of fast moving objects. As the deformations in the transformer have very low occurrence frequency (for example once in a year), the time interval (T_I) between transmitted pulses is not an important factor.

A typical transmitted pulse has been shown in Fig. 8 and its parameters have been listed in Table III.

Fig. 9 shows the timing of received pulses. If the test duration is T_d seconds, then N_r pulses can be sent, and we have:

$$N_r = \frac{T_d}{T_I}. \tag{1}$$

The total number of samples in each scan (N_C) is calculated, as follows:

$$N_C = \frac{T_C}{T_S} \tag{2}$$

where, T_S and T_C are the sampling time and receiving duration time in each scan, respectively.

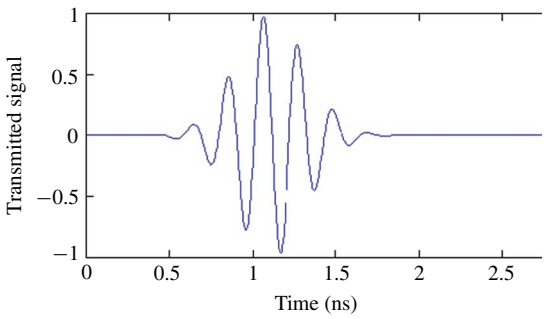

Fig. 8. Typical transmitted pulse.

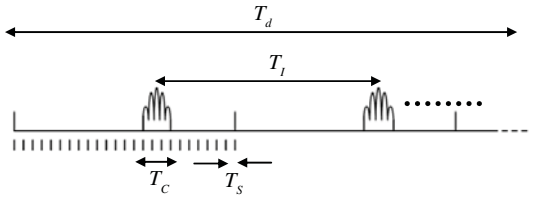

Fig. 9. Timing of pulses received in receiver.

IV. ON-LINE MONITORING OF RADIAL DEFORMATION

The first phase in on-line monitoring of transformer winding mechanical damages is the detection of deformations and displacements. In this phase, the measurements are classified in the following two groups.

1) Reference measurement: There is no deformation on the transformer winding model. The results of this test have been stored as a normal and base case.
2) Deformation measurement: Different radial deformations are applied to the winding but the test set-up configuration is the same as the reference case.

The radial deformation is detected by the comparison of reference and deformation measurements based on a proposed index.

In the second phase, the amount of the mechanical deformation is estimated for a possible maintenance. This is been accomplished by a regression tree [31] explained in Section VIII.

V. DETECTION OF RADIAL DEFORMATION

The analysis of the measured data, to detect radial deformations has two essential stages. The first stage is the selection of a window in the time axis and the second stage is the comparison of test results with the reference measurement using the mean absolute distance criteria.

A. Selection of Window by Using TOA Method

Only a part of the received signal is related to the transformer model and the rest are reflected signals, from the surrounding objects of transformer model. In the first stage, unwanted parts of the signal should be omitted by using TOA method by using the following steps.

Step 1: In this step, a matrix which has the data of received signals should be formed. The sampled data of each signal

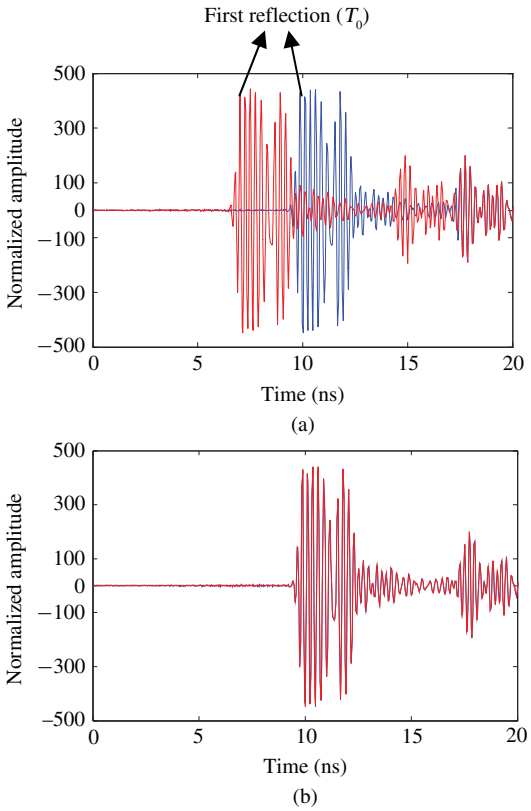

Fig. 10. Two received pulses (a) before and (b) after synchronization.

received in the test duration time (T_d), is placed in a row of this matrix. The number of the matrix columns is equal to the number of samples in each scan (N_C). The matrix has N_r rows, where N_r is the number of pulses, which have been sent in T_d seconds (test duration time). It can be said that for each test set-up configuration, the test has been repeated for N_r times and results of each test have been saved in a row. The results of the reference case (measurement) are stored in a matrix named w_1. The received pulses for the cases modeling the deformations are stored in the matrices w_2, w_3 and w_n, where (n–1) is the number of modeled deformations.

Step 2: Some of received pulses are pseudo noise which should be eliminated from the data matrices. This can be accomplished by deleting the out of range data.

Step 3: The received signals are not synchronized because of the timing jitter. Considering Fig. 6, the shortest distance between the transmitter and the receiver is equal to d_1. The first peak of the received signal waveform is related to the direct line of sight of the transmitter and receiver, as shown in Fig. 10(a). The instant of this peak determines the time origin (T_0). Based on this method, the time origin of the signal can be determined for each test. All of the received pulses in the reference measurement and deformation measurement are shifted to be synchronized with each other. Fig. 10(b) shows the signals after synchronization.

After synchronization of two data sets as shown in Fig. 10, the signal shape is found to be consistent in almost all of the scans. For the reduction of the remaining white noise, the data has been averaged as is mentioned in the next step.

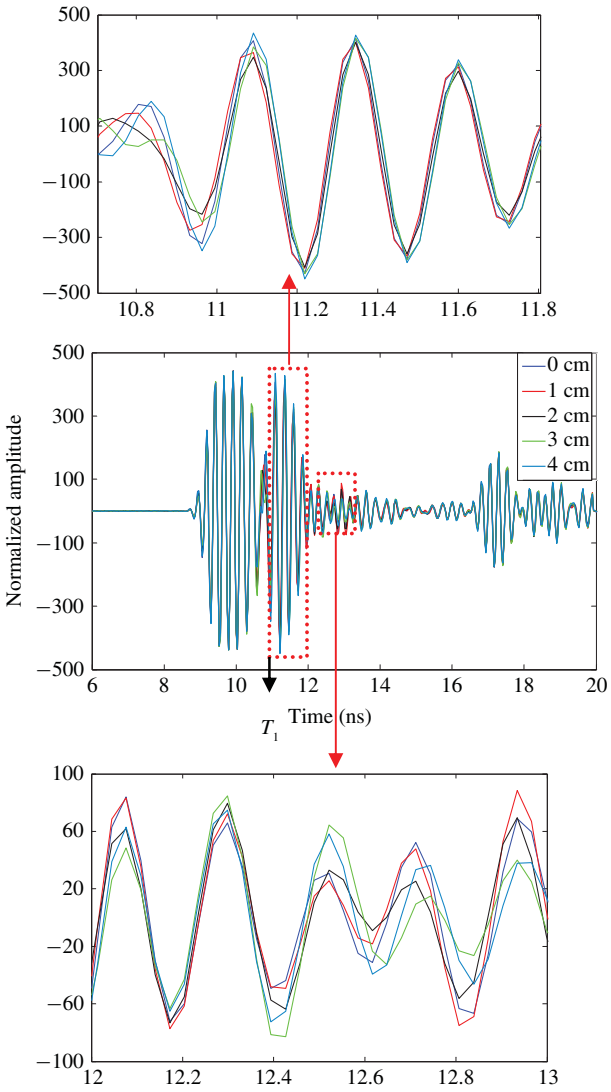

Fig. 11. Received pulse can be windowed to detect winding reflections.

Step 4: In the step 3, the time origin of all rows of the matrices, i.e., w_1, w_2, w_3, …, w_n have been determined. In this step, the columns of each matrix should be averaged to form a representative vector for each deformed case named, (W_1, W_2, W_3, …,W_n).

Step 5: Fig. 11 shows a sample of received pulses for the reference winding and deformed windings with a deformation area of 4 cm^2 and deformation length of 1 to 4 cm.

In this step, in order to decrease the size of the matrix, the time interval related to transformer winding reflections is determined in the received waveform. The distance between the antenna and the winding is known (d_3). So, the moment of the first reflection from the transformer winding is known. This parameter can be calculated by the following equation:

$$T_1 = \frac{2d_3 - d_1}{3 \times 10^8} \tag{3}$$

where, T_1 is the receiving time of the first reflection received from the model of the winding. In a real transformer, the propagation medium is oil. This will just affect the velocity of electromagnetic wave used in the denominator of equation

TABLE IV
PARAMETERS OF MEASUREMENT SET-UP

Parameter	T_C	T_I	T_s	T_d	d_4	d_3	d_2	d_1
Value	20 ns	50 ms	31.789 ps	5s	90 cm	50 cm	40 cm	60 cm

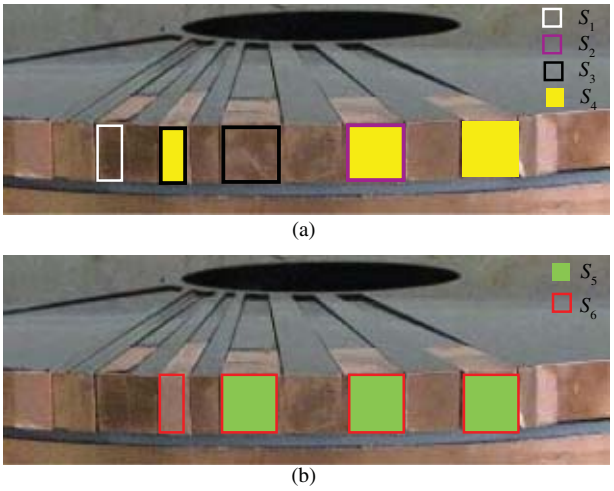

Fig. 12. Different combinations of sectors. (a) S_1, S_2, S_3, and S_4. (b) S_5 and S_6.

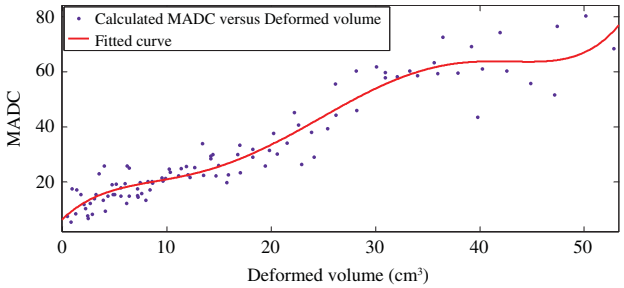

Fig. 13. Calculated *MADC* for first window versus deformed volume (cm^3).

(3), i.e. $u = 3 \times 10^8/\sqrt{\varepsilon_r}$, where ε_r is the relative dielectric constant of the oil. In a real transformer, the aging effect of the oil can be considered by regular measurements of the oil relative dielectric constant (ε_r).

Due to the very simple model, used for a transformer winding, there have been no multipath effects in our measurements. In a real transformer, however one should consider the multipath effects.

The timing interval of reflections (related to the winding) can be determined (using the winding dimensions) by the same equation. The part of the pulse related to the winding can be extracted from the received pulse for the reduction of unwanted reflections. Because of the existence of multipath, there are several reflections from the transformer winding. The second reflection is attenuated because its traveling time in the space is longer. The window related to the first and second winding reflections has been shown in Fig. 13. After windowing, the reduced size matrices are named $W_1^{'}$, $W_2^{'}$, $W_3^{'}, \ldots, W_n^{'}$.

TABLE V
DIFFERENT COMBINATIONS OF SECTORS

Cross Section No.	Deformation width (cm)× Deformation thickness (cm)	Cross Section Area (cm^2)
S_1	1×2	2
S_2	2×2	4
S_3	$1 \times 2 + 2 \times 2$	6
S_4	$2 \times 2 + 2 \times 2 + 1 \times 2$	10
S_5	$2 \times 2 + 2 \times 2 + 2 \times 2$	12
S_6	$2 \times 2 + 2 \times 2 + 2 \times 2 + 1 \times 2$	14

B. Comparison of Waveform of Each Test with Reference Case

After windowing, each pulse is compared with the reference case. The surrounding objects do not have any movement and only the deformation has been applied to the transformer winding. By using the Mean Absolute Distance Criterion (*MADC*), the signals received in different deformation tests ($W_2^{'}$, $W_3^{'}, \ldots, W_n^{'}$) can be compared with the signal of the reference case ($W_1^{'}$), as follows:

$$MADC(k) = \frac{1}{N} \sum_{j=T_1/T_s}^{T_2/T_s} \left| \frac{W_k'(j) - W_1'(j)}{W_1'(j)} \right|, \quad k = 2, \ldots, n \qquad (4)$$

where, T_1 is the beginning time of the window or receiving time of the first reflection from the transformer, T_2 is the end instant of the window and N is defined, as follows:

$$N = \frac{T_2 - T_1}{T_S} \qquad (5)$$

where, T_S is the sampling time.

VI. MEASUREMENT RESULTS OF RADIAL DEFORMATION

Table IV shows the measurement set-up parameters. Table V lists dimensions of different combinations of sectors and Fig. 12 shows different combination of sectors (highlighted in similar colors), which have been used to model different radial deformation extents.

The variation of the deformation length, as shown in Fig. 2(a), for each of cross sections is from 0 to 40 mm in 2 mm steps. Therefore, there are 120 different cases of radial deformation with different extents. The volume of deformation is calculated by multiplying the length, width and thickness of each sector and adding to the volume of other sectors in a specified cross section. The results of measurements of radial deformations are sorted according to the volume of deformation in ascending order.

The measurements of the radial deformation have been studied by using the proposed *MADC* index. Fig. 13 shows the calculated *MADC* for the first window ($T_1 = 10.169$ ns and $T_2 = 12.076$ ns) versus deformed volume and Fig. 14 shows

TABLE VI
FEATURES AND THEIR SYMBOLS EXTRACTED USING WAVELET

Magnitude		Phase		Power	
Feature	Symbol	Feature	Symbol	Feature	Symbol
$a_7(f_0{:}f_n)$	$X_1{:}X_{45}$	$a_7(f_0{:}f_n)$	$X_{361}{:}X_{405}$	a_7	X_{721}
$d_1(f_0{:}f_n)$	$X_{46}{:}X_{90}$	$d_1(f_0{:}f_n)$	$X_{406}{:}X_{450}$	d_1	X_{722}
$d_2(f_0{:}f_n)$	$X_{91}{:}X_{135}$	$d_2(f_0{:}f_n)$	$X_{451}{:}X_{495}$	d_2	X_{723}
$d_3(f_0{:}f_n)$	$X_{136}{:}X_{180}$	$d_3(f_0{:}f_n)$	$X_{496}{:}X_{540}$	d_3	X_{724}
$d_4(f_0{:}f_n)$	$X_{181}{:}X_{225}$	$d_4(f_0{:}f_n)$	$X_{541}{:}X_{585}$	d_4	X_{725}
$d_5(f_0{:}f_n)$	$X_{226}{:}X_{270}$	$d_5(f_0{:}f_n)$	$X_{586}{:}X_{630}$	d_5	X_{726}
$d_6(f_0{:}f_n)$	$X_{271}{:}X_{315}$	$d_6(f_0{:}f_n)$	$X_{631}{:}X_{675}$	d_6	X_{727}
$d_7(f_0{:}f_n)$	$X_{316}{:}X_{360}$	$d_7(f_0{:}f_n)$	$X_{676}{:}X_{720}$	d_7	X_{728}

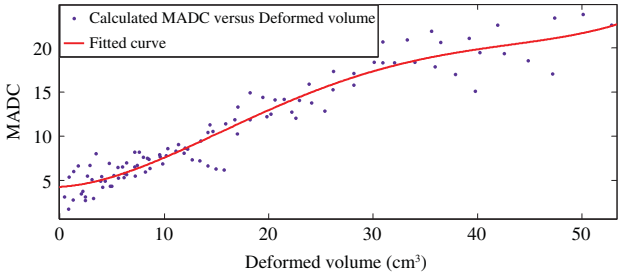

Fig. 14. Calculated *MADC* for second window versus deformed volume (cm^3).

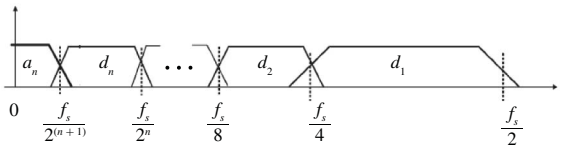

Fig. 15. Frequency ranges cover for details and final approximation.

the calculated *MADC* for the second window ($T_1 = 12.076$ ns and $T_2 = 13.983$ ns) versus deformed volume.

A curve can be fitted to the calculated *MADC* for both windows. The results of the curve fitting are, as follows.

For the first window:

$$f(x) = 4.239\text{e}-006 \cdot x^5 + -0.0005416 \cdot x^4 + 0.02353 \cdot x^3 + -0.3995 \cdot x^2 + 3.584 \cdot x + 6.43 \quad (6)$$

and, for the second window:

$$f(x) = 9.006\text{e}-006 \cdot x^4 + -0.001053 \cdot x^3 + 0.03569 \cdot x^2 + 0.06971 \cdot x + 4.293. \quad (7)$$

The *MADC* indexes are ascending functions of the deformed volume and they can approximately estimate the severity of the radial deformation using fitted curves. Considering *MADC* curves, presented in Figs. 13 and 14, it is obvious that they have not enough accuracy for finding the exact amount of radial deformations. But, they can be used to detect an existing radial deformation.

VII. ESTIMATION OF RADIAL DEFORMATION EXTENT

For the exact determination of the radial deformation extent, a regression tree can be trained by the features extracted from measurements of winding in different states. Then, the tree can estimate the amount of the radial deformation for an unknown state of the winding.

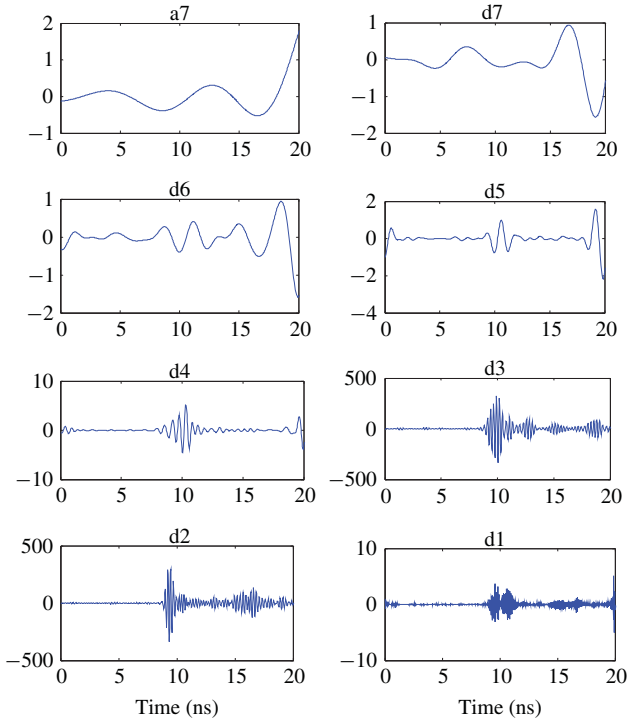

Fig. 16. Typical waveform of detail and approximate components of received signal for daubechies 16.

A. Feature Extraction Using Wavelet Transform

A wavelet-based signal processing technique [32], [33] is an effective tool for feature extraction. Some applications of the technique have been reported for data compression and fault detection [34]. The wavelet transform is the breaking up of a signal into scaled and shifted versions of the mother wavelet [35]. The wavelet function is localized in time and frequency yielding wavelet coefficients at different scales (levels). Any discrete signal $x[n]$ can be decomposed by using the wavelet function and the wavelet coefficients, as follows:

$$x[n] = \sum_k a_{j0,k}.2^{\frac{j0}{2}}.\phi[2^{j0}n - k] + \sum_{j=j0}^{J-1}\sum_k d_{j,k}.2^{\frac{j}{2}}.\varphi[2^j n - k] \quad (8)$$

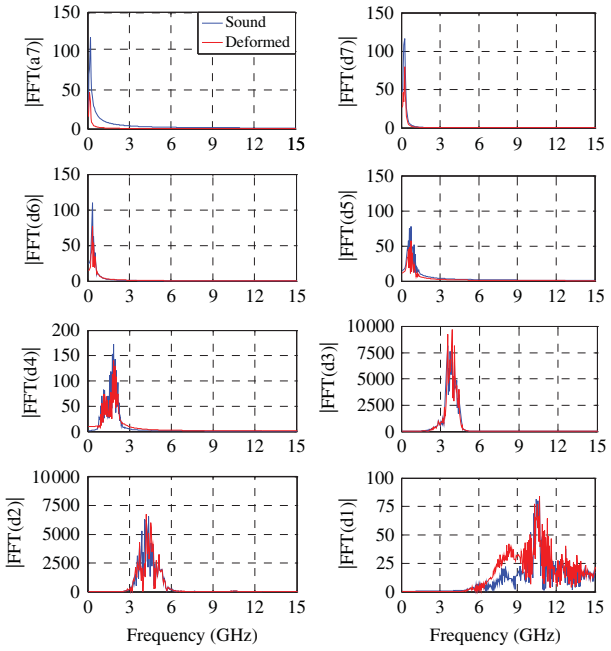

Fig. 17. Magnitude of FFT of details and approximation of two different received signal.

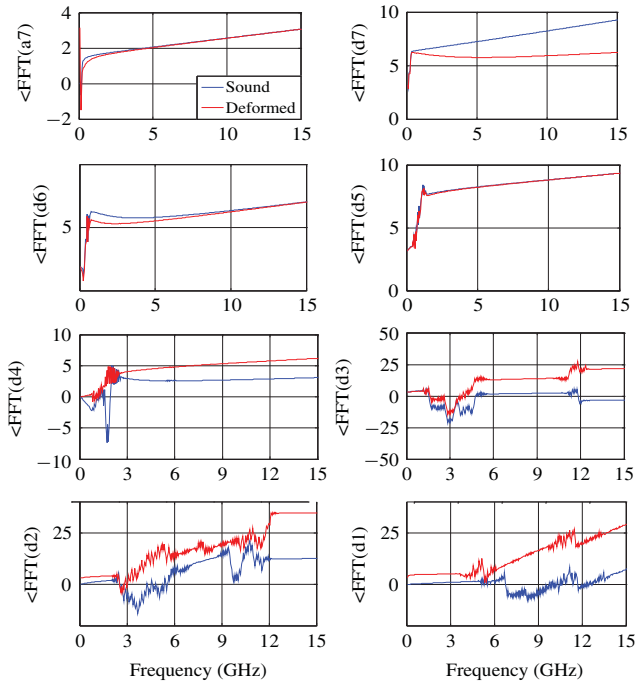

Fig. 18. Phase of FFT of details and approximation of two different received signal.

where ϕ[n] is the scaling function, and $\phi[n]$ is the mother wavelet, j is the scale of decomposition, k is the shifting factor, $a_{j0,k}$ are the approximation coefficients at a scale of $s = 2^{j0}$, $d_{j,k}$ are the detail coefficients at a scale of $s = 2^j$ and N is equal to 2^j, where N is the number of x samples.

The DWT divides the given function into different frequency components based on a power of two divisions. More concretely, if f_s (in samples per second) is the sampling rate used for capturing x, at the j'th decomposition level, the detail d_j and the approximation a_j coefficient contains the information concerning the original signal components with the frequency bandwidth $[f_s/2^{j+1}, f_s/2^j]$ and $[0, f_s/2^{j+1}]$, respectively [35], [36]. Therefore, DWT carries out the filtering process shown in Fig. 15. Note that the filtering is not ideal, a fact leading to a certain overlap between adjacent frequency bands. The shape of the frequency response for these filters depends on the type and the order of the mother wavelet used in the analysis.

Also, the type of wavelet function is important for the fault detection. Several wavelet functions such as daubechies 4, 8, 16, 28, 32, symlet 2, 4, 8, coiflet 3 have been tested for a typical radial deformation. It is shown that daubechies 16 maximizes the fault index for the detection of the radial deformation [37]. Therefore, daubechies 16 has been selected as the wavelet function to extract useful features. The approximate a_7 and details $d_1, \ldots, d_7$ for daubechies 16 mother wavelet are shown in Fig. 16.

After the decomposition of signals, the extraction of useful features is studied. The FFT is employed to feature extraction from the DWT. The corresponding phase and magnitude of FFT of the approximate a_7 and details $d_1, \ldots, d_7$ of the received signals for two different states of winding are shown in Figs. 17 and 18, respectively. For data reduction, only a small frequency range of the FFT magnitude is used. It is obvious that, the magnitude and the phase of FFT differ significantly for different types of fault. Thus, the features are the magnitude, the phase and the power of FFT of details and approximation of received signals, which are listed with their symbols in Table VI.

B. Regression Tree

Classification and regression tree (CART) is extensively implemented in machine fault diagnosis, for classification or regression problems depending on the response variable, which is either categorical or numerical [31]. Regression tree is applied to forecast the short-term load of the power system [38], [39].

A binary tree is developed for a regression problem with the repeated splits of subsets into two next subsets according to independent variables. The data must be as homogenous as possible with respect to the response variables, in order to produce subsets of the data by the regression tree. The trees, which are produced by CART, consist of internal nodes and terminal nodes or leaf nodes. Each internal node is related to a decision function to show the next node, while each terminal node is the output of a given input vector that leads to this node [40].

Both classification and regression trees built by CART consist of the tree growing and pruning.

Suppose L be a learning sample of size n, and it consists of n couples of observations $(y_1, x_1), \ldots, (y_n, x_n)$, where $x_i = (x_{1i}, \ldots, x_{di})$ is a set of independent variables and $y_i \in R$ is a response associated with x_i [41]. In this paper, y_i is a specific case of the radial deformation and x_i is the feature vector for this case. To prepare the training set, the sector S_2 has been

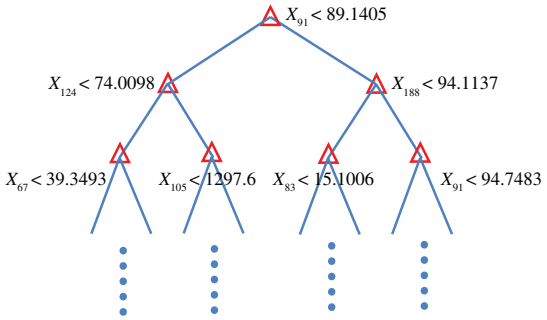

Fig. 19. Regression tree for estimation of radial deformation extent.

TABLE VII
CART TEST RESULTS

Deformation (mm)	Estimated deformation (mm)	Absolute error (mm)
2	2	0
4.5	4.5	0
7	7.5	0.5
9.5	10	0.5
12	12	0
14.5	14	0.5
17	17.5	0.5
19.5	20	0.5

moved in steps of 0.5 mm from 0 to 20 mm. Therefore, there are 41 different cases of the radial deformation with different extents.

The aim of the regression tree is to predict the values of response variables $y = (y_1, \ldots, y_n)$ derived from the set of independent variables $(x_1, \ldots, x_n)$. To build the tree, the learning sample L is partitioned into two subsets by a binary split. The splits are formed by using the inequality condition between the criterion and value of independent variables. The result of this splitting is to move the couples (y, x) to the left or right nodes, which contain more homogeneous responses. This process is repeated until the terminal nodes are achieved. The CART can inherently estimate the suitability of features for the separation of objects, representing different classes and regressions. The occurrence of a feature in a tree provides the information about the importance of the associated feature. This facility can be directly exploited for the purpose of the important feature selection. It is clear that the top node is the best node for regression. The other features in the nodes of CART appear in descending order of importance. Fig. 19 shows the regression tree for the estimation of the radial deformation extent, which has been created by using MATLAB Statistics Toolbox.

It can be seen that the most important feature is X_{91}, (the top node of Fig. 19). In the second level, X_{124} and X_{188} are the important ones. The tree is tested by 8 test samples. The regression tree test results are listed in Table VII.

The minimum detectable radial deformation is very important, because the tolerances are very fine for the transformer and deformations more than 1% can cause serious damages to the winding. So, it is important to detect the deformations below 1%. The minimum detectable radial deformation using the proposed method is 0.66 % of the winding radius, i.e., 2 mm. But, the minimum detectable radial deformation in the outer HV winding using FRA method is 5% of the transformer winding radius [42]. The algorithm of the estimation of the radial deformation extent is shown in Fig. 20.

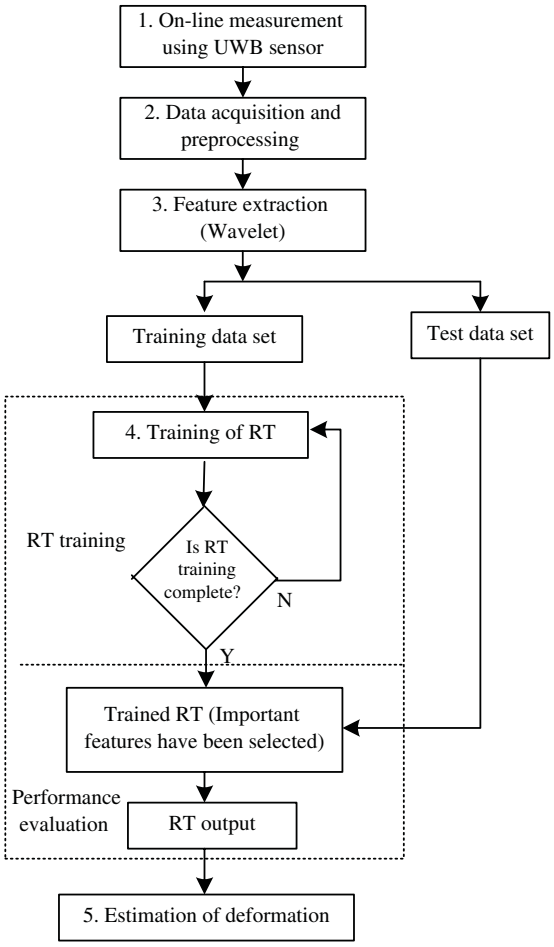

Fig. 20. Algorithm for estimation of radial deformation extent.

In the first step, a databank of reflected signals for the sound and deformed cases are acquired using UWB sensors. Preprocessing the data is accomplished in the second step. This step comprises the steps 1–4 presented in Section VI of the paper. In the third step, the feature extraction from the data is performed by the wavelet transform. The output is divided to training and test data sets. In the fourth step, training of the Regression Tree (RT) is performed by using the training data set. In the fifth step, the performance evaluation of the RT is accomplished by the estimation of the radial deformation of the test data set.

VIII. CONCLUSION

On-line monitoring of transformer winding radial deformation using UWB sensors has been proposed in this paper. The measurements on a simplified model of the transformer winding show the sensitivity of the proposed method to the winding deformation. In the paper, an index has been proposed, which can be used to detect the radial deformation. The radial deformation extents have been estimated using regression tree by features extracted from wavelet transform of measured signal.

REFERENCES

[1] A. Gandhi, T. Corrigan, and L. Parsa, "Recent advances in modeling and online detection of stator interturn faults in electrical motors," *IEEE Trans. Ind. Electron.*, vol. 58, no. 5, pp. 1564–1575, May 2011.

[2] M. Wang, A. J. Vandermaar, and K. D. Srivastava, "Review of condition assessment of power transformers in service," *IEEE Electr. Insul. Mag.*, vol. 18, no. 6, pp. 12–25, Nov.–Dec. 2002.

[3] D. K. Xu and J. H. Huang, "On-line monitoring of winding deformation of power transformer," in *Proc. IEEE Conf. Electr. Insul. Mater.*, Himeji, Japan, Nov. 2001, pp. 853–856.

[4] A. S. Morched, L. Marti, R. H. Brierly, and J. G. Lackey, "Analysis of internal winding stresses in EHV generator step-up transformer failures," *IEEE Trans. Power Del.*, vol. 11, no. 2, pp. 888–894, Apr. 1996.

[5] J. Christian and K. Feser, "Procedures for detecting winding displacements in power transformers by the transfer function method," *IEEE Trans. Power Del.*, vol. 19, no. 1, pp. 214–220, Jan. 2004.

[6] E. Rahimpour, J. Christian, K. Feser, and H. Mohseni, "Transfer function method to diagnose axial displacement and radial deformation of transformer windings," *IEEE Trans. Power Del.*, vol. 18, no. 2, pp. 493–505, Apr. 2003.

[7] W. Chen, C. Sun, Y. Yun, and Z. Xie, "Study on the recognition of transformer winding deformation by using wavelet transform in the LVI method," in *Proc. Int. Conf. Power Syst. Technol.*, vol. 3. 2002, pp. 1966–1969.

[8] T. Leibfried and K. Feser, "Monitoring of power transformers using the transfer function method," *IEEE Trans. Power Del.*, vol. 14, no. 4, pp. 1333–1341, Aug. 2002.

[9] T. Leibfried and K. Feser, "Off-line and on-line monitoring of power transformers using the transfer function method," in *Proc. IEEE Int. Symp. Electr. Insul.*, Montreal, QC, Canada, Jun. 1996, pp. 34–111.

[10] T. Leibfried and K. Feser, "On-line monitoring of transformers by means of the transfer function method," in *Proc. IEEE Int. Symp. Electr. Insul.*, Pittsburgh, PA, Jun. 1994, pp. 111–114.

[11] S. Tenbohlen, F. Stril, and P. Mayer, "Experience-based evaluation of benefits of on-line monitoring systems for power transformers," in *Proc. CIGRE Sess.*, Paris, France, 2002, pp. 12–110.

[12] M. A. Hejazi, G. B. Gharehpetian, and A. Mohammadi, "Characterization of on-line monitoring of transformer winding axial displacement using electromagnetic waves," in *Proc. 15th Int. Symp. High Voltage Eng.*, Ljubljana, Slovenia, Aug. 2007, pp. 27–31.

[13] M. A. Hejazi, G. B. Gharehpetian, and A. Mohammadi "On-line monitoring of radial deformation of transformer winding using scattering parameters," in *Proc. 15th Int. Symp. High Voltage Eng.*, Ljubljana, Slovenia, Aug. 2007, pp. 27–31.

[14] M. A. Hejazi, G. B. Gharehpetian, G. R. Moradi, M. Mohammadi, and H. A. Alehoseini, "Application of classifiers for on-line monitoring of transformer winding axial displacement by electromagnetic NDT," *Electr. Power Compon. Syst.*, vol. 39, no. 4, pp. 387–403, Apr. 2011.

[15] M. A. Hejazi, G. B. Gharahpetian, R. Farajidana, G. R. Moradi, M. Mohammadi, and H. A. Alehoseini, "A new on-line monitoring method of transformer winding axial displacement based on measurement of scattering parameters and decision tree," *J. Expert Syst. Appl.*, vol. 38, no. 7, pp. 8886–8893, Jul. 2011.

[16] M. A. Hejazi, G. B. Gharehpetian, G. Moradi, H. A. Alehosseini, and M. Mohammad, "Online monitoring of transformer winding axial displacement and its extent using scattering parameters and k-nearest neighbour method," *IET Generat., Transmiss. Distribut.*, vol. 5, no. 8, pp. 824–832, Aug. 2011.

[17] *Federal Communications Commission*, Standard 02-48, Feb. 2002.

[18] Z. Sahinoglu, S. Gezici, and I. Guvenc, *Ultrawideband Positioning Systems: Theoretical Limits, Ranging Algorithms, and Protocols*. Cambridge, U.K.: Cambridge Univ. Press, 2008.

[19] I. I. Immoreev and D. V. Fedotov, "Ultrawideband radar systems: Advantages and disadvantages," in *Proc. IEEE Ultrawideband Syst. Technol. Conf.*, Baltimore, MD, May 2002, pp. 201–205.

[20] G. F. Ross, "A historic review of UWB radar and communications and future directions," presented at the IEEE Radio and Wireless Conference, Boston, MA, Oct. 2003.

[21] J. Park and C. Nguyen, "An ultrawide-band microwave radar sensor for nondestructive evaluation of pavement subsurface," *IEEE Sensors J.*, vol. 5, no. 5, pp. 942–949, Oct. 2005.

[22] H. Soganci, S. Gezici, and H. V. Poor, "Accurate positioning in ultrawideband systems," *IEEE Wireless Commun.*, vol. 18, no. 2, pp. 19–27, Apr. 2011.

[23] S. Hantscher and C. G. Diskus, "Pulse-based radar imaging using a genetic optimization approach for echo separation," *IEEE Sensors J.*, vol. 9, no. 3, pp. 271–276, Mar. 2009.

[24] R. J. Fontana "Recent system applications of short-pulse ultrawideband (UWB) technology," *IEEE Trans. Microw. Theory Tech.*, vol. 52, no. 9, pp. 2087–2104, Sep. 2004.

[25] M. D. Judd and L. I. B. B. Y. Hunter, "Partial discharge monitoring of power transformers using UHF sensors. Part I: Sensors and signal interpretation," *IEEE Electr. Ins. Mag.*, vol. 21, no. 2, pp. 5–14, Mar.–Apr. 2005.

[26] M. D. Judd, L. Yang, and I. B. B. Hunter, "Partial discharge monitoring for power transformer using UHF sensors. Part 2: Field experience," *IEEE Electr. Ins. Mag.*, vol. 21, no. 3, pp. 5–13, May–Jun. 2005.

[27] M. A. Hejazi, J. Ebrahimi, G. B. Gharehpetian, R. Faraji-Dana, and M. Dabir, "Feasibility studies on on-line monitoring of transformer winding mechanical damage using UWB sensors," in *Proc. ICEM 19th Int. Conf. Electr. Mach.*, Rome, Italy, Sep. 2010, pp. 1–6.

[28] G. Mokhtari, M. A. Hejazi, and G. B. Gharehpetian, "Simulation of On-line monitoring of transformer winding axial displacement using UWB waves," in *Proc. ICEM 19th Int. Conf. Electr. Mach.*, Rome, Italy, Sep. 2010, pp. 6–8.

[29] G. Mokhtari, G. B. Gharehpetian, R. Faraji-dana, and M. A. Hejazi, "On-line monitoring of transformer winding axial displacement using UWB sensors and neural network," *Int. Rev. Electr. Eng.*, vol. 5, no. 5, pp. 2122–2128, Oct. 2010.

[30] J. Ebrahimi, G. B. Gharehpetian, H. Amindavar, and M. A. Hejazi, "Antennas positioning for On-line monitoring of transformer winding radial deformation using UWB sensors," in *Proc. Int. Conf. Power Energy*, Kuala Lumpur, Malaysia, Nov.–Dec. 2010, pp. 352–356.

[31] L. Breiman, J. H. Friedman, R. A. Olshen, and C. J. Stone, *Classification and Regression Trees*, New York: Chapman & Hall, 1984.

[32] R. R. Coifman and M. V. Wickerhauser, "Entropy-based algorithms for best basis selection," *IEEE Trans. Inf. Theory*, vol. 38, no. 2, pp. 713–718, Mar. 1992.

[33] Y. Meyer, *Wavelets and Applications*. New York: Springer-Verlag, 1992.

[34] S. Santoso, E. J. Powers, and W. M. Grady, "Power quality disturbance data compression using wavelet transform methods," *IEEE Trans. Power Del.*, vol. 12, no. 3, pp. 1250–1257, Jul. 1997.

[35] *The Wavelet Tutorial* [Online]. Available: http://users.rowan.edu/~polikar/wavelets/wttutorial.html

[36] J. Antonino-Daviu, M. Riera-Guasp, J. Roger-Folch, and M. P. Molina, "Validation of a new method for the diagnosis of rotor bar failures via wavelet transformation in industrial induction machines," *IEEE Trans. Ind. Appl.*, vol. 42, no. 4, pp. 990–996, Jul.–Aug. 2006.

[37] J. Ebrahimi, G. B. Gharehpetian, H. Amindavar, and M. A. Hejazi, "Detection of transformer winding radial deformations by using UWB pulses and DWT," in *Proc. Int. Conf. Power Energy*, Kuala Lumpur, Malaysia, Nov.–Dec. 2010, pp. 369–372.

[38] J. Yang and J. Stenzel, "Short-term load forecasting with increment regression tree," *J. Elect. Power Syst. Res.*, vol. 76, nos. 9–10, pp. 880–888, Jun. 2006.

[39] H. Moti, N. Kosemura, K. Ishiguro, and T. Kondo, "Short-term load forecasting with fuzzy regression tree in power systems," in *Proc. IEEE Int. Conf. Syst., Man, Cybern.*, vol. 3. Tucson, AZ, Aug. 2002, pp. 1948–1953.

[40] M. Sugeno, G. T. Kang, "Structure identification of fuzzy model," *J. Fuzzy Sets Syst.*, vol. 28, no. 1, pp. 15–33, Oct. 1988.

[41] V. T. Tran, B.-S. Yang, M.-S. Oh, and A. C. C. Tan, "Fault diagnosis of induction motor based on decision trees and adaptive neurofuzzy inference," *J. Exp. Syst. Appl.*, vol. 36, no. 2, pp. 1840–1849, 2009.

[42] P. Karimifard, G. B. Gharehpetian, and S. Tenbohlen, "Localization of winding radial deformation and determination of deformation extent using vector fitting based estimated transfer function," *J. Eur. Trans. Electr. Power*, vol. 19, no. 5, pp. 749–762, Jul. 2009.

Maryam Sadat Akhavan Hejazi received the B.Sc. degree in electrical engineering and the M.Sc. and Ph.D. degrees in electric power engineering from the Amirkabir University of Technology, Tehran, Iran, in 2003, 2006, and 2011, respectively.

She is currently an Assistant Professor with the University of Kashan, Kashan, Iran. She is the author of more than 30 journal and conference papers. Her current research interests include transformer monitoring, modeling, distributed generation, and smart grids.

Javad Ebrahimi (S'10) was born in Isfahan, Iran, in 1986. He received the B.Sc. degree in electrical engineering from the University of Tabriz, Tabriz, Iran, in 2008, and the M.S. degree (first class honors) in electrical engineering from the Amirkabir University of Technology (AUT), Tehran, Iran, in 2010. He is currently pursuing the Ph.D. degree with the Electrical Engineering Department, AUT.

His current research interests include the analysis and control of power electronic converters, flexible alternative current transmission systems devices, distributed generation, and transformer monitoring.

Gevork B. Gharehpetian (SM'08) received the Ph.D. degree (first class honors) in electrical engineering from the University of Tehran, Tehran, Iran, in 1996.

He was an Assistant Professor with the Amirkabir University of Technology, Tehran, from 1997 to 2003, an Associate Professor from 2004 to 2007, and has been a Professor since 2007. He was selected by the ministry of higher education as the Distinguished Professor of Iran and the Iranian Association of Electrical and Electronics Engineers (IAEEE) as the Distinguished Researcher of Iran. He is the author of more than 450 journal and conference papers. His current research interests include power systems, transformers transients, and power electronics applications in power systems.

Prof. Gharehpetian was awarded the National Prize in 2008 and 2010, respectively. He is a Distinguished Member of IEEE and IAEEE, respectively, and a member of the Central Board of IAEEE.

Mohammad Mohammadi was born in Shiraz, Iran, in 1977. He received the B.Sc. degree from Shiraz University, Shiraz, in 2000, and the M.Sc. and Ph.D. degrees from the Amirkabir University of Technology (AUT), Tehran, Iran, in 2002 and 2007, respectively, all in electrical engineering.

He is currently with Shiraz University. He is the author of more than 40 journal and conference papers. His current research interests include power system security assessment, machine learning, and power system dynamics.

Reza Faraji-Dana received the B.Sc. degree (with honors) from the University of Tehran, Tehran, Iran, in 1986, and the M.Sc. and Ph.D. degrees from the University of Waterloo, Waterloo, ON, Canada, in 1989 and 1993, respectively, all in electrical engineering.

He was a Post-Doctoral Fellow with the University of Waterloo for one year. In 1994, he joined the School of Electrical and Computer Engineering, University of Tehran, where he is currently a Professor. He has been engaged in several academic and executive responsibilities, among which was his deanship of the Faculty of Engineering for more than four years until 2002, when he was elected as the University President by the university council. He was the President of the University of Tehran until December 2005. He is the author of several technical papers published in reputable international journals and refereed conference proceedings.

Prof. Faraji-Dana is an Associate Member of the Iran Academy of Sciences. He was the Chairman of the IEEE-Iran Section from 2007 to 2009. He received the Institution of Electrical Engineers Marconi Premium Award in 1995.

Gholamreza Moradi received the B.Sc. degree from the University of Tehran, Tehran, Iran, the M.Sc. degree from the Iran University of Science and Technology, Tehran, and the Ph.D. degree from the Amirkabir University of Technology (AUT), Tehran, all in electrical engineering.

He was with Civil Aviation of Technology as a Faculty Member from 1997 to 2006, then he joined AUT, where he is an Associate Professor in the Electrical Engineering Department. He is the co-author of five books and numerous papers in his research fields. His current research interests include microwave measurements, numerical measurements, radio frequency circuits, and system designs.